JOURNAL OF Materials CHEMISTRY

# Structural and transport characteristics of the LAMOX family of fast oxide-ion conductors, based on lanthanum molybdenum oxide $La_2Mo_2O_9$†

**F. Goutenoire,*[a] O. Isnard,[b] E. Suard,[c] O. Bohnke,[a] Y. Laligant,[a] R. Retoux[a] and Ph. Lacorre[a]**

[a]*Laboratoire des Fluorures, UPRES-A CNRS 6010, Université du Maine, 72085 Le Mans Cedex 9, France. E-mail: francois.goutenoire@univ-lemans.fr*
[b]*Laboratoire de Cristallographie, BP 166, 38042 Grenoble Cedex 9, France*
[c]*Institut Laue-Langevin, BP156X, 38042 Grenoble Cedex 9, France*

***Received 11th May 2000, Accepted 30th June 2000***
***First published as an Advance Article on the web 5th October 2000***

A new family of fast $O^{2-}$ conductors, which exhibit anionic conductivity comparable to that of stabilised zirconia, is presented. The parent compound of this new family, hereafter called LAMOX, is lanthanum molybdate $La_2Mo_2O_9$. Various substitutions have been attempted: on the lanthanum site $(La_{2-x}A_x)Mo_2O_9$ with A = Sr, Ba, K, or Bi; on the molybdenum site $La_2(Mo_{2-x}B_x)O_9$ with B = Re, S, W, Cr and V; and on the oxygen site with fluorine. Most of these substitutions suppress the phase transition which occurs in $La_2Mo_2O_9$ around 580 °C from a low temperature α form to a high temperature (more conducting) β form, and stabilise the β form at room temperature. Several members of the LAMOX series are studied through X-ray and neutron diffraction, and conductivity measurements. Large $O^{2-}$ thermal factors and local static disorder agree well with the anionic nature of the conductivity. Partly vacant sites with short inter-site distances suggest a most probable conduction path with tridimensional character.

## 1 Introduction

Fast oxide-ion conductors attract considerable interest for both fundamental and technical reasons, due to their important fields of application, among which solid oxide fuel cells, oxygen sensors, or oxygen pumping devices (see, for instance, recent reviews such as refs. 1 and 2, and references therein). The main oxide-ion conductors known to date belong to four distinct structural groups: fluorite type (stabilised zirconia,[3] ceria, δ-$Bi_2O_3$,[4,5]...), deficient perovskites[6] (doped $LaGaO_3$[7,8] or browmillerite phases), Aurivillius type phases (BIMEVOX),[9,10] pyrochlores[11] ($Gd_2Zr_2O_7$, $Gd_2Ti_2O_7$).[12] Among those, the most famous and commonly used materials are stabilised zirconia.[3]

Given the widespread interest of such materials, any new finding on the topic should stimulate research in the field, with the aim to increase anionic conductivity at lower temperature. Here we present a new family of fast oxide-ion conductors: the LAMOX series, based on atomic substitutions on the parent compound $La_2Mo_2O_9$.[13,14] The most probable conduction path in $La_2Mo_2O_9$ is deduced from its crystallographic arrangement (Section 2), and the extension (Section 3) and conduction properties (Section 4) of the LAMOX family are explored through several ionic substitutions.

## 2 Parent compound $La_2Mo_2O_9$

We have recently discovered[13,14] a new family of fast oxide-ion conductors whose parent compound is lanthanum molybdate $La_2Mo_2O_9$, which exhibits a transition from a slightly distorted low temperature α form, to a cubic high temperature β form. It is accompanied by an abrupt increase by almost two orders of magnitude of the anionic conductivity (see Fig. 1). Above this transition, which takes place around 580 °C, the oxide-ion conductivity is slightly higher than that of yttria-stabilized zirconia, the reference compound in the field.

### 2.1 Crystal structure of β-$La_2Mo_2O_9$

Neutron powder diffraction patterns were recorded at two temperatures (620 °C and 670 °C) on Bragg–Brentano X-ray diffractometers and/or on the Debye–Scherrer neutron diffractometers D2B (ILL) and D1B (CRG-CNRS instrument operating at the ILL). These patterns were collected under the following conditions: angular range 12.5°–91.85°, step 0.2°, wavelength 1.28 Å, total counting time 12 hours on D1B, and angular range 0°–160°, step 0.05°, wavelength 1.59 Å, for 6 hours on D2B. All measurements were recorded under air in a silica glass container. Fourier syntheses and structural refinements were calculated and refined with programs FullProf and ShelxL93.[15,16]

The electron diffraction study was performed on a 200 kV side entry JEOL 2010 electron microscope with a double tilt specimen holder operated at room temperature.

In our previous structural study based on the D1B pattern,[14] four different models were tested, the most consistent one appearing to be model D, with three oxygen sites O1, O2 and O3, and a slight cationic deficiency ($La_{3.556}Mo_{3.556}O_{16} = La_2Mo_2O_9$). The result of the new refinements using the D2B data, with about 24% more reflections, is in agreement with the previous arrangement (see Table 1, and Fig. 2(a) for final refinement).

As shown in reference 14, the crystal structure of β-$La_2Mo_2O_9$ appears to be very close to that of β-$SnWO_4$,[17] with extra oxygen atoms in statistical occupation (see Table 1). Cations occupy the same type of positions in both compounds, as well as most anions (see Fig. 3). Given that divalent tin is a lone pair element the tungstate formula can be rewritten $Sn_2W_2O_8E_2$ (E = lone pair). In this case, trivalent lanthanum with no lone pair replaces divalent tin and its lone pair, which is partially replaced by oxygen, so that the formulation of the lanthanum molybdate becomes $La_2Mo_2O_{8+1}\square$. The created vacancy (□) is indeed a favourable

†Basis of a presentation given at Materials Discussion No. 3, 26–29 September, 2000, University of Cambridge, UK.

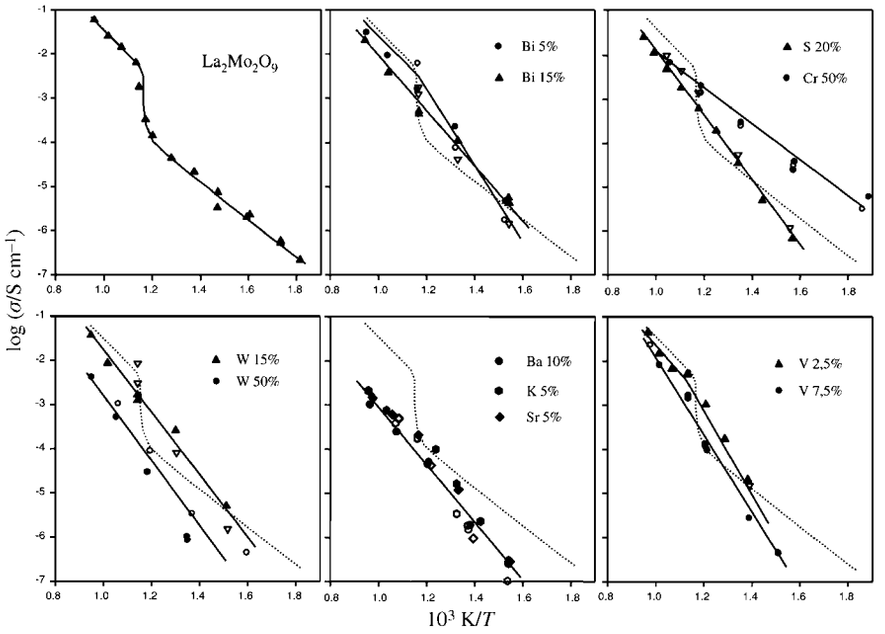


**Fig. 1** Arrhenius plot of the conductivity of pure and substituted $La_2Mo_2O_9$, upon heating (solid symbols) and cooling (open symbols).

element for the extra oxygen migration, as evidenced by the anionic conductivity of the molybdate. As a structural proof, it can be seen on Fig. 3 that the extra oxygen atom partially occupies, in the molybdate, the site normally occupied by the tin lone pair in the tungstate. Besides, the large anisotropic values of oxygen thermal factors, and the undulation of the neutron diffraction background (see Fig. 4, with a first maximum around $Q=3.1$ Å$^{-1}$ characteristic of a minimal O–O distance around 2.5 Å, according to the Debye formula) are further indications of the oxygen disordering.

Concerning the crystal structure of the low temperature form α-$La_2Mo_2O_9$, we have already mentioned[14] that it is a $2\times3\times4$ superstructure of the cubic form with a slight (probably monoclinic) distortion.

### 2.2 Conduction path in $La_2Mo_2O_9$

It is to be noted that 2 of the 3 oxygen sites of β-$La_2Mo_2O_9$ are partially occupied (O2 and O3), which represent 3/4 of the total number of oxygen atoms, and as many vacancies. Oxygen atoms O2 and O3 are thus most probably the only ones which participate in the conduction path, since oxygen site O1, despite it also having a large thermal factor, appears to remain fully occupied. It can be made even clearer when considering the shortest distances between oxygen sites. Since sites O2 and O3 are together 50% occupied, and site O3 less than 50%, some O2–O3 and O3–O3 distances (see Table 2) are smaller than the commonly admitted smallest O–O distance (about 2.5 Å). When such is the case, it means that one of the two sites is not occupied by an oxygen atom, and that the oxygen atom on the other site is therefore very close to a vacancy. These shortest O2–O3 and O3–O3 distances are thus indicative of the most likely conduction path for oxide ions. Fig. 5a gives a view of such short distances between sites O2 and O3. They form interconnected infinite paths along the 3-fold axes of the cubic structure, whose approximate trace is schematised by cylindrical rods on Fig. 5b, which thus most likely represent the oxide-ion conduction path in $La_2Mo_2O_9$. This conduction path is three-dimensional in nature, by virtue of the rods interconnection in a cubic symmetry.

**Table 1** Crystallographic parameters of β-$La_2Mo_2O_9$ (670 °C) and *$La_{1.7}Bi_{0.3}Mo_2O_9$* (25 °C)

| Model<br>Formula | | β-$SnWO_4$<br>$SnWO_4$ | Model A<br>$La_2Mo_2O_8$ | *Model A*<br>*$La_{1.7}Bi_{0.3}$-$Mo_2O_8$* | Model B<br>$La_2Mo_2O_9$ | *Model B*<br>*$La_{1.7}Bi_{0.3}$-$Mo_2O_9$* | Model C<br>$La_2Mo_2O_8$ | *Model C*<br>*$La_{1.7}Bi_{0.3}$-$Mo_2O_8$* | Model D<br>$La_2Mo_2$-$O_9$ | *Model D*<br>*$La_{1.7}Bi_{0.3}$-$Mo_2O_9$* |
|---|---|---|---|---|---|---|---|---|---|---|
| La/*Bi* (4a) | *x* | 0.8416(2) | 0.8514(3) | *0.8522(4)* | 0.8517(3) | *0.8532(3)* | 0.8492(4) | *0.8525(3)* | 0.8525(3) | *0.8519(3)* |
| Sn (4a) | Occupancy | 1 | 1 | *1* | 1 | *1* | 1 | *1* | 0.889 | *0.889* |
| | $B_{eq}$/Å$^{2a}$ | 0.96(2) | 4.6(3) | *3.8(3)* | 5.2(2) | *5.2(2)* | 5.9(2) | *5.4(2)* | 5.9(2) | *5.0(3)* |
| Mo (4a) | *x* | 0.1644(1) | 0.1776(5) | *0.1649(7)* | 0.1684(6) | *0.1700(4)* | 0.1665(5) | *0.1673(5)* | 0.1695(5) | *0.1689(5)* |
| W (4a) | Occuppancy | 1 | 1 | *1* | 1 | *1* | 1 | *1* | 0.889 | *0.889* |
| | $B_{eq}$/Å$^{2a}$ | 0.69(2) | 4.2(2) | *5.4(3)* | 4.4(2) | *2.7(2)* | 5.6(2) | *3.9(2)* | 4.4(2) | *3.4(3)* |
| O1 (4a) | *x* | 0.3039(16) | 0.333(2) | *0.3137(7)* | 0.3144(6) | *0.3142(6)* | 0.3141(5) | *0.3138(6)* | 0.3179(6) | *0.3171(5)* |
| | Occupancy | 1 | 1 | *1* | 1 | *1* | 1 | *1* | 1 | *1* |
| | $B_{eq}$/Å$^{2a}$ | 1.60(36) | 14.23(2) | *3.5(3)* | 6.8(15)[b] | *6.7(2)*[b] | 9.0(2) | *9.4(2)* | 8.4(2) | *8.5(2)* |
| O2 (12b) | *x* | 0.0470(18) | 0.9855(4) | *0.9802(4)* | 0.9864(5) | *0.9828(5)* | 0.9797(6) | *0.9796(5)* | 0.9908(6) | *0.9916(7)* |
| | *y* | 0.1362(19) | 0.1537(9) | *0.149(2)* | 0.177(1) | *0.1710(9)* | 0.166(2) | *0.168(1)* | 0.179(1) | *0.177(2)* |
| | *z* | 0.2271(18) | 0.3287(8) | *0.311(2)* | 0.334(1) | *0.3363(9)* | 0.329(1) | *0.3328(8)* | 0.337(1) | *0.336(1)* |
| | Occupancy | 1 | 1 | *1* | 0.87(1) | *0.97(1)* | 0.77(1) | *0.85(1)* | 0.66(2) | *0.66(9)* |
| | $B_{eq}$/Å$^{2a}$ | 2.02(23) | 10.25(4) | *18.6(2)* | 9.2(4) | *10.7(3)* | 12.2(4) | *11.6(4)* | 6.7(5) | *5.7(4)* |
| O3 (12b) | *x* | | | | 0.919(2) | *0.920(2)* | 0.920(2) | *0.907(1)* | 0.912(2) | *0.906(2)* |
| | *y* | | | | 0.613(3) | *0.604(2)* | 0.608(2) | *0.610(1)* | 0.648(4) | *0.667(4)* |
| | *z* | | | | 0.550(2) | *0.546(2)* | 0.549(2) | *0.5482(8)* | 0.544(2) | *0.548(1)* |
| | Occupancy | | | | 0.29(1) | *0.18(1)* | 0.23(1) | *0.15(1)* | 0.34(2) | *0.34(9)* |
| | $B_{eq}$/Å$^{2a}$ | | | | 8.0(5) | *0.0(2)* | 4.5(2) | *−1.1(3)* | 18.4(1) | *26.5(1)* |
| *R* Bragg (%) | | 3.4[c] | 12.6 | *14.2* | 6.1 | *8.94* | 6.4 | *9.21* | 5.7 | *8.01* |

[a] $B_{iso}=4/3a^2$ $(\beta_{11}+\beta_{22}+\beta_{33})$. [b] Isotropic *B* thermal factors. [c] From reference 17, single crystal data.

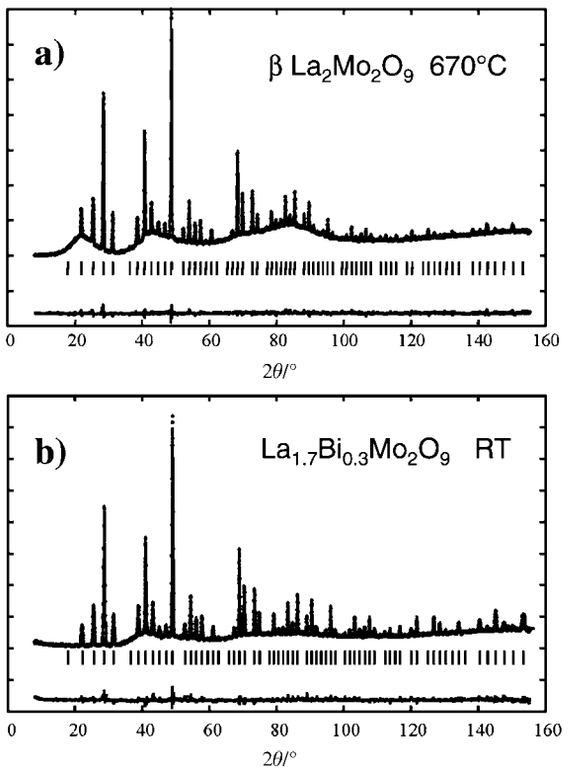


**Fig. 2** D2B neutron diffraction pattern fits (model D) of the crystal structure of: a) β-$La_2Mo_2O_9$ at 670 °C. Note that the strong undulating background is in this case due to diffuse scattering from the glass container. b) $La_{1.7}Bi_{0.3}Mo_2O_9$ at room temperature. In this case the strong undulating background is due to the sample. Dots = observed patterns; lines = calculated patterns; below = difference pattern.

## 3 Synthesis and crystallographic characterisation in the LAMOX family

### 3.1 Synthesis

Various substitutions on both cationic sites of $La_2Mo_2O_9$ were carried out: $(La_{2-x}M_x)Mo_2O_9$ (M = Sr, Ba, K, Bi) and $La_2(Mo_{2-x}M_x)O_9$ with (M = Re, S, W, Cr and V) were prepared from appropriate stoichiometric mixtures of starting materials $La_2O_3$, $MoO_3$, $SrCO_3$, $BaCO_3$, $K_2CO_3$, $Bi_2O_3$, $ReO_3$, $La_2(SO_4)_3$, $WO_3$, $La_2CrO_6$ or $V_2O_5$. In the case of Sr, Ba, K, Bi, S, W and V the weighted powder was mixed in an agate mortar, and then placed in an alumina crucible. These mixtures were first heated in air at 500 °C for 12 hours, then kept at 700–1100 °C (depending on the substituted cation, see Table 3) for several hours, and finally cooled down slowly. Several regrindings and heatings were necessary in order to obtain a pure compound. In the case of rhenium substitution the mixed powder was placed in a sealed platinum tube. The tube was first heated slowly at 500 °C for a few hours, then the temperature was slowly increased to 900 °C and kept at this temperature for 12 hours. In the case of chromium substitution the weighted powder was placed in an alumina crucible and heated under a flow of pure oxygen firstly at 500 °C and then at 700 °C for a few hours.

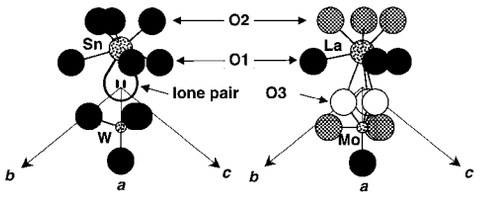


**Fig. 3** Cationic environments in β-$SnWO_4$ (left) and β-$La_2Mo_2O_9$ (right). For clarity, the environment of La is limited to the nearest neighbours. Hatched and open circle oxygen sites are partially occupied.

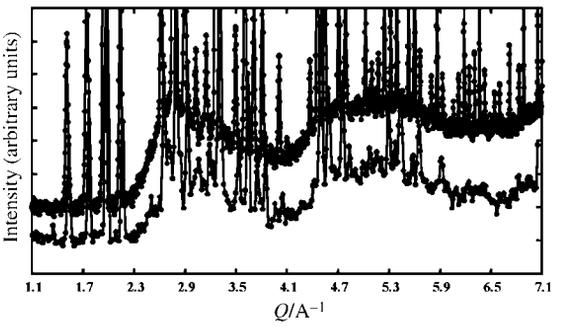


**Fig. 4** Detail of the neutron diffraction patterns of β-$La_2Mo_2O_9$ (below) and $La_{1.7}Bi_{0.3}Mo_2O_9$ (above) at room temperature *versus* $Q = 4\pi \sin\theta/\lambda$, showing a large diffuse peak in the background around 3.1 $Å^{-1}$ (due to short range order with pair distances around 2.5 Å). Note that the container contribution to the background is negligible (vanadium container). For clarity, the patterns have been shifted with respect to each other.

Partial substitution of oxygen by fluorine was successfully attempted: $La_2Mo_2O_{8.95}F_{0.1}$ was prepared from an appropriate stoichiometric mixture of starting materials $La_2O_3$, LaOF and $MoO_3$. The synthesis conditions were identical to those of the rhenium substituted compound.

### 3.2 Crystal structure of $La_{1.7}Bi_{0.3}Mo_2O_9$

Partial substitution of lanthanum by bismuth in $La_2Mo_2O_9$ leads to a stabilisation at room temperature of the cubic form, as evidenced by electron diffraction (see Fig. 6). The results of the structure refinement from the room temperature neutron diffraction pattern (D2B) of $La_{1.7}Bi_{0.3}Mo_2O_9$ is given in Table 1 (see also Fig. 2b). The agreement between the calculated and observed patterns is not as good as those of the high temperature form of $La_2Mo_2O_9$. For instance, the equivalent isotropic thermal factors for O3 in models B, C and D seem unrealistic. This is probably related to the (re)introduction of a lone pair among O3 oxygen atoms (see Fig. 3).

**Table 2** Selected bond distances (Å) for β-$La_2Mo_2O_9$ (model D, $T = 670$ °C)[a]

| | |
|---|---|
| La polyhedron | |
| La–O2 | 2.496(5) [×3][b] |
| La–O3 | 2.71(2) [×3][b] |
| La–O1 | 2.696(4) [×3] |
| La–O3 | 2.83(3) [×3][b] |
| La–O2 | 2.809(7) [×3][b] |
| Mo polyhedron | |
| Mo–O3 | 1.73(4) [×3][b] |
| Mo–O2 | 1.77(3) [×3][b] |
| Mo–O1 | 1.83(2) [×1] |
| Oxygen–oxygen short distances | |
| O1–O2 | 2.574(7) [×3][b] |
| O1–O2 | 2.789(8) [×3][b] |
| O1–O3 | 2.79(2) [×3][b] |
| O2–O3 | 2.30(2) [×1][b] |
| O2–O3 | 2.86(2) [×1][b] |
| O2–O3 | 2.68(2) [×1][b] |
| O2–O3 | 1.54(3) [×1][b] |
| O2–O3 | 2.98(2) [×1][b] |
| O3–O3 | 1.74(2) [×2][b] |

[a]Crystallographic parameters: space group $P2_13$ (no. 198), $Z = 2$, $a = 7.2342(1)$ Å, $R_{Bragg} = 5.7\%$, $R_p = 23.5\%$, $R_{wp} = 11.3\%$, $R_{exp} = 8.5\%$, $\chi^2 = 1.8$, number of reflections = 156, number of refined parameters = 35. [b]O2 and O3 sites are partially occupied.

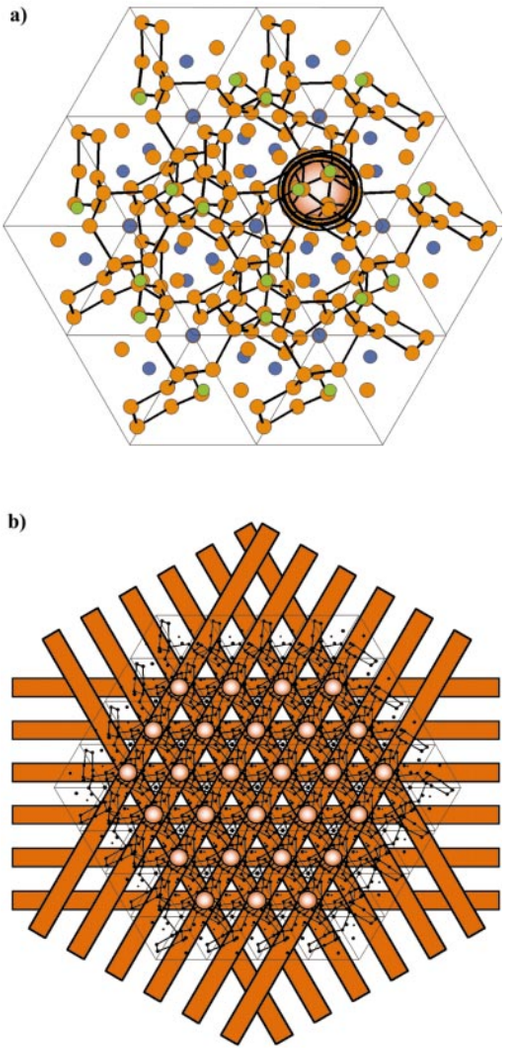


**Fig. 5** Conduction path in $La_2Mo_2O_9$: (a) 3D lattice of short O2–□ and O3–□ distances in β-$La_2Mo_2O_9$ forming infinite paths along the [111] cubic direction (direction of the projection). Orange = oxygen, blue = lanthanum, green = molybdenum; (b) 3D lattice of the conduction paths schematised as infinite cylindrical rods along the cube diagonals (see section on Fig. 5a).

Attempts to find another oxygen position from Fourier difference analysis in model A were in vain. It seems that the strict localisation of the extra oxygen is a real challenge (such a difficulty to locate conducting ions is rather common in ionic conductors due to their strong delocalisation).[18,19] One can note the same undulation in the backgrounds of the neutron diffraction patterns of $La_{1.7}Bi_{0.3}Mo_2O_9$ and α-$La_2Mo_2O_9$ at room temperature (see Fig. 4).

**Table 3** Synthesis temperature and RT cell parameters of members of the LAMOX family; for α-$La_2Mo_2O_9$ the single cell parameters have been averaged to pseudo cubic. Estimated standard deviations for the cell parameter are below 0.0005 Å (except for $La_2Mo_2O_9$)

| Compounds | Temperature /°C | *a*/Å |
|---|---|---|
| α-$La_2Mo_2O_9$ | 850–900 | ≈7.149 |
| K(5%) | 960 | 7.1718 |
| Ba(10%) | 970 | 7.1878 |
| Sr(5%) | 1050 | 7.1680 |
| Cr(50%) | 700 | 7.1315 |
| W(15%) | 1000 | 7.1524 |
| W(50%) | 1100 | 7.1535 |
| W(75%) | 1100 | 7.1526 |
| W(80%) | 1100 | 7.1402 |
| Bi(5%) | 850 | 7.1643 |
| Bi(10%) | 850 | 7.1757 |
| Bi(15%) | 850 | 7.1862 |
| S(20%) | 800 | 7.0784 |
| S(50%) | 800 | 7.1460 |
| V(2.5%) | 900 | 7.1500 |
| V(7.5%) | 900 | 7.1480 |
| Re(5%) | 900 | 7.1567 |

### 3.3 Cell parameter evolution upon substitution

Several other substitutions on the cationic sites of $La_2Mo_2O_9$ have been tested, all of them leading to a stabilisation of the cubic form at room temperature. The cell parameter evolutions with the percentage and the nature of the substitution are summarised in Fig. 7 and Table 3. The parameter evolution can be simply analysed by considering the cationic sizes[20] (for instance with 9-fold and tetrahedral coordination for La and Mo substitutes, respectively). Substitutions on the lanthanum site $(La_{2-x}A_x)Mo_2O_9$ (A = Sr, K, Bi) give coherent results in view of the ionic radii $r(Sr^{II})_9 = 1.31$ Å, $r(K^{I})_9 = 1.55$ Å and $r(La^{III})_9 = 1.216$ Å. The size of $Bi^{III}$ is comparable to that of $La^{III}$, but we should take into account the presence of the lone pair, which can explain the large increase of cell parameter upon doping. Substitutions on the molybdenum site $La_2(Mo_{2-x}B_x)O_9$ with B = S, W, Cr and V give a cell parameter evolution which also reflects the ionic radii: $r(S^{VI})_4 = 0.12$ Å, $r(W^{VI})_4 = 0.42$ Å, $r(Cr^{VI})_4 = 0.26$ Å, $r(V^{V})_4 = 0.355$ Å, and $r(Mo^{VI})_4 = 0.41$ Å. The substitutions with sulfur and chromium could be performed up to at least fifty percent, and in the case of tungsten up to eighty percent.

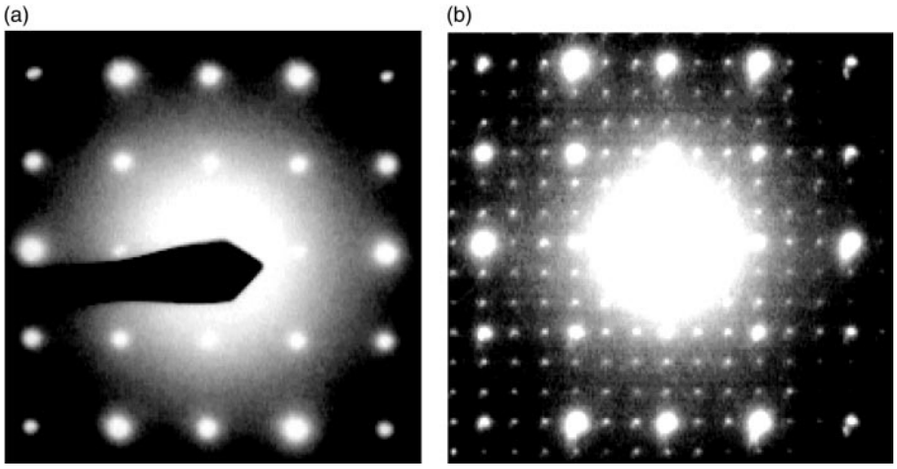


**Fig. 6** Room temperature electron diffraction patterns of: (a) $La_{1.7}Bi_{0.3}Mo_2O_9$ (cubic cell). (b) $La_2Mo_2O_{8.95}F_{0.1}$ showing a superstructure relative to the cubic cell.

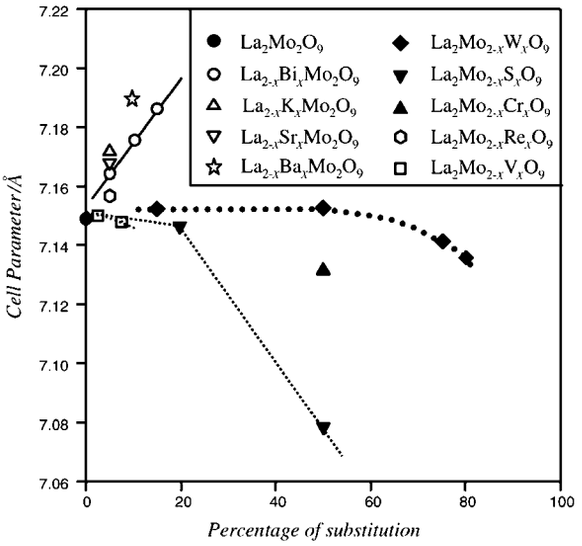


**Fig. 7** Evolution upon substitution rate of the cell parameters of different members of the LAMOX family. For α-$La_2Mo_2O_9$ the cell parameters have been averaged to pseudo cubic. Lines are guides for the eye.

Substitution by fluorine on the oxygen lattice leads to another type of superstructure, different from that of α-$La_2Mo_2O_9$ with a tripling of cubic cell parameters and a slight distortion (see Fig. 6).

## 4 Oxide-ion conduction in the LAMOX family

For conductivity measurements, gold or platinum electrodes were vacuum deposited on both flat surfaces of rod shaped samples (about 5 mm in diameter and 6 mm in length). These rods were prepared from appropriate powder samples. Approximately three drops of a solution of polyvinyl alcohol were mixed with 1 g of as-synthesized powder in an agate mortar. This mixture was placed in a furnace for a few hours at 200 °C, and then pressed in a die under about 1–2 tons. These rod shaped samples were first heated slowly in air at 400 °C for a few hours, then kept at 700–1100 °C (depending on the substitution) for several hours, and finally cooled down slowly. The ratios of the measured density (deduced from the weight and geometric parameters of the samples) to the theoretical density ranged from 70 to 80%

The conductivity was determined by impedance spectroscopy in the 0.1 Hz–32 MHz range using a Schlumberger Solartron SI1260 frequency response analyser. Each set of data was recorded under dry air flow at the given temperature after 1 h stabilisation. The conductivity of substituted compounds given at 500 and 800 °C (Table 4), were obtained from a linear regression of conductivity measured during heating and cooling of the sample.

**Table 4** The conductivities of substituted compounds

| Compounds | $\sigma$/S cm$^{-1}$ ($T$ = 500 °C) | $\sigma$/S cm$^{-1}$ ($T$ = 800 °C) |
|---|---|---|
| α-$La_2Mo_2O_9$ | $4.6\times10^{-5}$ | — |
| β-$La_2Mo_2O_9$ | — | $8.02\times10^{-2}$ |
| K (5%) | $1.40\times10^{-5}$ | $5.65\times10^{-3}$ |
| Ba (10%) | $8.56\times10^{-6}$ | $2.74\times10^{-3}$ |
| Sr (5%) | $1.20\times10^{-5}$ | $6.03\times10^{-3}$ |
| Cr (50%) | $5.42\times10^{-4}$ | $9.98\times10^{-3}$ |
| W (15%) | $1.77\times10^{-4}$ | $6.04\times10^{-2}$ |
| W (50%) | $9.33\times10^{-6}$ | $4.21\times10^{-3}$ |
| Bi (5%) | $2.05\times10^{-4}$ | $6.96\times10^{-2}$ |
| Bi (15%) | $1.33\times10^{-4}$ | $2.22\times10^{-2}$ |
| S (20%) | $1.01\times10^{-4}$ | $4.81\times10^{-2}$ |
| V (2.5%) | $3.00\times10^{-5}$ | $5.20\times10^{-2}$ |

As previously reported,[13,14] $La_2Mo_2O_9$ is a good oxide-ion conductor, as can be seen on Fig. 1 which presents an Arrhenius plot of its conductivity as deduced from impedance measurements. The phase transition around 580 °C is accompanied, upon heating, by an abrupt increase of the conductivity by almost two orders of magnitude. In all cases of substitution (Sr, Ba, K, Bi, S, W, Cr and V) no phase transition was observed from conductivity measurements (see Fig. 1).

In most cases the conductivity of the substituted compounds is of the same order as that of $La_2Mo_2O_9$. For Bi (5%), W (15%) and V (2.5%) substitutions, the conductivity at 800 °C is very close to that of β-$La_2Mo_2O_9$ (see Table 4). In the case of bismuth doping, the large cell parameter increase does not improve anionic conduction probably due to the introduction of the bismuth lone-pair in the conduction path, which tends to block conduction rather than to open the lattice. For Ba (10%), K (5%) and Sr (5%) substitutions, the conductivity at 800 °C is almost one order of magnitude lower than that β-$La_2Mo_2O_9$ (see Table 4). The comparison of the conductivity of the substituted compounds and α-$La_2Mo_2O_9$ at 500 °C presents an interesting feature in the case of Cr (50%): the chromium substitution is the only case where the conductivity below the transition is one order of magnitude higher than that of α-$La_2Mo_2O_9$ in the whole temperature range (see Fig. 1).

## 5 Conclusion

We have presented in this paper a new family of fast oxide-ion conductors called LAMOX and based on parent compound $La_2Mo_2O_9$. Several members of this family, obtained by partial substitution on the different ionic sites, have been studied through X-ray and neutron diffraction, and conductivity measurements. The structural characterisation from powder samples suffers from the low number of uncorrelated diffraction peaks. A more accurate localisation of oxygen atoms, together with a better characterisation of physical properties would necessitate single crystals, whose growth attempts are currently under consideration. The partial substitution of oxygen by fluorine gives another promising research field, since fluorine doping is a way to modulate the rate of vacancies on the anionic sublattice. These different fields are currently under study and will be thoroughly explored in the near future. On a more general point of view, the substitution of a lone pair element could lead to a fruitful concept for the elaboration of other families of oxide-ion conductors, and open new fields of research. It will be fully developed in a subsequent paper.[21]

## References

1 B. C. H. Steele, *Oxygen ion conductors* in *High Conductivity Solid Ionic Conductors, Recent Trends and Applications*, ed. T. Takahashi, World Scientific Publishing Co., Singapore, 1989, pp. 402–446.
2 J. C. Boivin and G. Mairesse, *Chem. Mater.*, 1998, **10**, 2870.
3 E. C. Subbarao, *Zirconia—an overview in Advances in Ceramics*, eds. A. H. Heuer and L. W. Hobbs, vol. 3, Science and Technology of Zirconia I, American Ceramic Society, Columbus, OH, 1981, pp. 1–24.
4 T. Takahashi and H. Iwara, *J. Appl. Electrochem.*, 1973, **3**, 65.
5 H. A. Harwig and A. G. Gerards, *J. Solid State Chem.*, 1978, **26**, 265.
6 K. R. Kendall, C. Navas, J. K. Thomas and H.-C. zur Loye, *Solid State Ionics*, 1995, **82**, 215.
7 T. Ishihara, H. Matsuda and Y. Takita, *J. Am. Chem. Soc.*, 1994, **116**, 3801.
8 M. Feng and J. B. Goodenough, *Eur. J. Solid State Inorg. Chem.*, 1994, **31**, 663.

9 F. Abraham, M. F. Debreuille-Gresse, G. Mairesse and G. Nowogrocki, *Solid State Ionics*, 1988, **28–30**, 529.
10 F. Abraham, J. C. Boivin, G. Mairesse and G. Nowogrocki, *Solid State Ionics*, 1990, **40–41**, 934.
11 H. L. Tuller, *Solid State Ionics*, 1997, **94**, 63.
12 S. A. Kramer and H. L. Tuller, *Solid State Ionics*, 1995, **82**, 15.
13 Ph. Lacorre, F. Goutenoire, O. Bohnke, R. Retoux and Y. Laligant, *Nature*, 2000, **404**, 856.
14 F. Goutenoire, O. Isnard, R. Retoux and Ph. Lacorre, *Chem. Mater.*, in press.
15 J. Rodriguez-Carvajal, *Fullprof*, version 3.5d, 1998.
16 ShelxS86, G. M. Sheldrick, in *Crystallographic Computing 3*, eds. G. M. Sheldrick, C. Krüger and R. Goddards, Oxford University Press, Oxford, 1985; G. M. Sheldrick, *ShelxL93*, A Program for Refinement of Crystal from Diffraction Data, University of Göttingen, 1993.
17 W. Jeitschko and A. W. Sleight, *Acta Crystallogr., Sect. B*, 1972, **28**, 3174.
18 M. J. Cooper and M. Sakata, *Acta Crystallogr., Sect. A*, 1979, **35**, 989.
19 C. Muller, M. Anne, M. Bacman and M. Bonnet, *J. Solid State Chem.*, 1998, **141**, 241.
20 R. D. Shannon, *Acta Crystallogr., Sect. A*, 1976, **32**, 751.
21 Ph. Lacorre, in preparation.